*Inorg. Chem.* **2006**, *45*, 10636–10641

# $^{19}F$ High Magnetic Field NMR Study of $\beta$-$ZrF_4$ and $CeF_4$: From Spectra Reconstruction to Correlation between Fluorine Sites and $^{19}F$ Isotropic Chemical Shifts

**C. Legein,*,† F. Fayon,‡ C. Martineau,† M. Body,§ J.-Y. Buzaré,§ D. Massiot,‡ E. Durand,|| A. Tressaud,|| A. Demourgues,|| O. Péron,† and B. Boulard†**

*Laboratoire des Oxydes et Fluorures, CNRS UMR 6010, Laboratoire de Physique de l'Etat Condensé, CNRS UMR 6087, Institut de Recherche en Ingénierie Moléculaire et Matériaux Fonctionnels, CNRS FR 2575, Université du Maine, Avenue Olivier Messiaen, 72085 Le Mans Cedex 9, France, Centre de Recherche sur les Matériaux à Haute Température, CNRS UPR 4212, 1D Avenue, Recherche Scientifique, 45071 Orléans Cedex 2, France, and Institut de Chimie de la Matière Condensée de Bordeaux, CNRS UPR 9048, 87 Avenue du Dr. A. Schweitzer, 33608 Pessac Cedex, France*

Received July 19, 2006

High magnetic field and high spinning frequency one- and two-dimensional one-pulse MAS $^{19}F$ NMR spectra of $\beta$-$ZrF_4$ and $CeF_4$ were recorded and reconstructed allowing the accurate determination of the $^{19}F$ chemical shift tensor parameters for the seven different crystallographic fluorine sites of each compound. The attributions of the NMR resonances are performed using the superposition model for $^{19}F$ isotropic chemical shift calculation initially proposed by Bureau et al. (Bureau, B.; Silly, G.; Emery, J.; Buzaré, J.-Y. *Chem. Phys.* **1999**, *249*, 85–104). A satisfactory reliability is reached with a root-mean-square (rms) deviation between calculated and measured isotropic chemical shift values equal to 1.5 and 3.5 ppm for $\beta$-$ZrF_4$ and $CeF_4$, respectively.

## Introduction

$^{19}F$ magic angle spinning (MAS) solid-state NMR can provide important structural information on the environment of fluorine atoms in ordered and disordered crystals, as well as amorphous materials through $^{19}F$ isotropic chemical shift measurements. Because of the increasing MAS speed and magnetic field, it is now possible to discriminate close isotropic peaks on the experimental spectra. The challenge is now to perform a reliable attribution of the $^{19}F$ NMR resonances to fluorine atoms. In numerous studies,[1−10] the attribution of the resonances was based on rough empirical correlations related to experimental observations that similar $^{19}F$ isotropic chemical shift values indicate similar local environments.

Bureau et al.[11] proposed an improvement hereafter called the superposition model, which assigns isotropic chemical shifts to fluorine crystallographic sites through the use of phenomenological parameters. This model was successfully applied to compounds from the $BaF_2-AlF_3$ and $CaF_2-AlF_3$ binary systems:[12] a refinement of the phenomenological parameters led to the attribution of $^{19}F$ NMR resonances to fluorine sites with a root-mean-square (rms) value equal to 6 ppm, allowing a predictive use of this model.[13] To assign

* To whom correspondence should be addressed. E-mail: christophe.legein@univ-lemans.fr.
† Laboratoire des Oxydes et Fluorures, Université du Maine.
‡ Centre de Recherche sur les Matériaux à Haute Température.
§ Laboratoire de Physique de l'Etat Condensé, Université du Maine.
|| Institut de Chimie de la Matière Condensée de Bordeaux.

(1) Miller, J. M. *Prog. Nucl. Magn. Reson. Spectrosc.* **1996**, *28*, 255−281.
(2) Bureau, B.; Silly, G.; Buzaré, J.-Y.; Emery, J.; Legein, C.; Jacoboni, C. *J. Phys.: Condens. Matter* **1997**, *9*, 6719−6736.
(3) Bureau, B.; Silly, G.; Buzaré, J.-Y.; Jacoboni, C. *J. Non-Cryst. Solids* **1999**, *258*, 110−118.
(4) Stebbins, J. F.; Zeng, Q. *J. Non-Cryst. Solids* **2000**, *262*, 1−5.
(5) Zeng, Q.; Stebbins, J. F. *Am. Mineral.* **2000**, *85*, 863−867.
(6) Chan, J. C. C.; Eckert, H. *J. Non-Cryst. Solids* **2001**, *284*, 16−21.
(7) Kiczenski, T. J.; Stebbins, J. F. *J. Non-Cryst. Solids* **2002**, *306*, 160−168.
(8) Youngman, R. E.; Dejneka, M. J. *J. Am. Ceram. Soc.* **2002**, *85*, 1077−1082.
(9) Kiczenski, T. J.; Du, L.-S.; Stebbins, J. F. *J. Non-Cryst. Solids* **2004,** *337*, 142−149.
(10) Youngman, R. E.; Sen, S. *Solid State Nucl. Magn. Reson.* **2005**, *27*, 77−89.
(11) Bureau, B.; Silly, G.; Emery, J.; Buzaré, J.-Y. *Chem. Phys.* **1999**, *249*, 85−104.
(12) Body, M.; Silly, G.; Legein, C.; Buzaré, J.-Y. *Inorg. Chem.* **2004**, *43*, 2474−2485.



10.1021/ic061339a CCC: $33.50 
Published on Web 11/22/2006

the NMR peaks to fluorine sites in $\beta$-$ZrF_4$ and $CeF_4$, we have applied, for the first time, the superposition model on basic fluorides containing several inequivalent fluorine sites.

$CeF_4$[14] and $\beta$-$ZrF_4$[15] are isostructural and are both involved in numerous material science applications. Fluorozirconate glasses[16] have retained considerable attention over the past few years due to their physical and optical properties.[17−20] Very recently, in the context of preparing glass−ceramic-based integrated optical amplifiers for the C telecom band, Boulard et al. have studied $\beta$-$ZrF_4$−$LaF_3$−$ErF_3$ vitreous films obtained by vapor-phase deposition.[21] Indeed, rare-earth doped transparent fluorozirconate glass ceramics with a high degree of crystallinity have been recently reported.[22] These materials are very promising in the field of integrated optics because they allow high erbium concentration (6−8 mol %) and higher absorption and emission cross-sections of erbium relative to that of the glassy host. Redox properties of Ce-based materials are used in catalytic devices developed for the post-combustion process for Ce-based oxides[23] or the oxidative coupling of methane in the case of $CeO_2$/$CaF_2$ system[24] since cerium is a regulator of the oxygen partial pressure over the catalyst. Moreover, the unique optical characteristics of ceria, its band gap around 3.1 eV, and the low value of refractive index around 2.05 suggest also that $CeO_2$ can be used as an UV absorber.[25] To characterize the structure of zirconium- and cerium-based fluoride compounds, we have studied in a first step crystalline $\beta$-$ZrF_4$ and $CeF_4$ by $^{19}$F solid-state NMR. $^{19}$F NMR studies of such crystalline phases are most of the time required prior the determination of the short-range structure and the assignment of fluorine environments in $ZrF_4$-based glasses and glass ceramics as well as in cerium IV- and fluorine-based materials.

We present here what are apparently the first $^{19}$F solid-state NMR data for $CeF_4$. $\beta$-$ZrF_4$ was recently studied by this technique at 11.7 T, but the assignement of the NMR resonances to the fluorine sites was not complete.[10]

In this work, we have obtained $^{19}$F MAS NMR spectra of $\beta$-$ZrF_4$ and $CeF_4$ at a very high magnetic field (17.6 T) and very high spinning frequency. Since these $^{19}$F MAS NMR spectra recorded at a high magnetic field show numerous intense spinning sidebands, we have used the two-dimensional one-pulse (TOP) processing[28] to obtain $^{19}$F "infinite spinning frequency" isotropic spectra, which allows a direct quantification of the unequivalent fluorine sites in the structure and is an alternative to the simulation of the spinning sideband manifolds. Structural data are presented for both studied compounds, which allow us to perform a partial attribution of the NMR resonances on the basis of their relative intensities. Finally, we show that the superposition model, initially proposed by Bureau et al.,[11] can be successfully applied to these compounds, leading to the assignment of the $^{19}$F resonances to the seven unequivalent fluorine sites present in the structure for each studied compound.

## Experimental Procedures

$\beta$-$ZrF_4$ was obtained from Astron. The product was characterized with powder X-ray diffraction (XRD); the X-ray powder pattern was compared to the one reported in the Powder Diffraction File (PDF) number 00-033-1480, confirming the presence of the $\beta$-phase only.

$CeF_4$ samples were prepared by fluorination of highly divided $CeO_2$ with $F_2$ gas at $T = 400-500$ °C. The samples were characterized with powder X-ray diffraction (XRD); the X-ray powder patterns were compared to the one reported in the Powder Diffraction File (PDF) number 04-007-3514, confirming the purity of the samples.

$^{19}$F one- and two-dimensional one-pulse MAS NMR spectra were recorded on an Avance 750 Bruker spectrometer operating at 17.6 T ($^{19}$F Larmor frequency of 705.85 MHz), using a 2.5 mm CP-MAS probehead. All spectra were acquired using a Hahn echo sequence with an inter-pulse delay equal to one rotor period. For $\beta$-$ZrF_4$, a 1.5 $\mu$s 90° pulse and a 3 $\mu$s 180° pulse were used, corresponding to a $^{19}$F nutation frequency of 170 kHz. As the $CeF_4$ spectrum extended over more than 600 kHz, shorter pulse durations (0.5 and 0.75 $\mu$s) were used, with the same $^{19}$F nutation frequency, to ensure a homogeneous irradiation of the whole spectrum. The complete irradiation of the spectra was carefully checked by recording spectra with various offsets. The discrimination of isotropic peaks from spinning sidebands was achieved by recording spectra at various spinning frequencies from 24 to 34 kHz. The recycle delay was set to 20 and 10 s for $\beta$-$ZrF_4$ and $CeF_4$, respectively, to ensure no saturation. The $^{19}$F chemical shifts are referenced to $CFCl_3$ at 0 ppm.

The processing of these $^{19}$F MAS spectra with extensive spinning sidebands manifold was carried out carefully, ensuring that all Fourier transforms start at $t = 0$. The two-dimensional one-pulse[26−28] (TOP) MAS spectra were reconstructed by stacking subspectra shifted by the spinning frequency from the conventional one-dimensional MAS spectra. Interpolation inside the one-dimensional spectrum when extracting subspectra was used to eliminate acquisition timing constraints.[28] The $^{19}$F isotropic "infinite spinning rate" MAS spectra were then obtained from the full

(13) Body, M.; Silly, G.; Legein, C.; Buzaré, J.-Y.; Calvayrac, F.; Blaha, P. *J. Solid State Chem.* **2005**, *178*, 3655−3661.
(14) Schmidt, R.; Mueller, B. G. *Z. Anorg. Allg. Chem.* **1999**, *625*, 605−608.
(15) Burbank, R. D.; Bensey, F. N., Jr. *USAEC Rep.* **1956**, *K-1280*, 1−19.
(16) Poulain, M.; Poulain, M.; Lucas, J. *Mater. Res. Bull.* **1975**, *10*, 243−246.
(17) Lucas, J. *J. Mater. Sci.* **1989**, *24*, 1−6.
(18) Adam, J. L. *Chem. Rev.* **2002**, *102*, 2461−2476.
(19) Leroy, D.; Lucas, J.; Poulain, M.; Ravaine, D. *Mater. Res. Bull.* **1978**, *13*, 1039−1046.
(20) Hasz, W. C.; Wang, J. H.; Moynihan, C. T. *J. Non-Cryst. Solids* **1993**, *161*, 127−132.
(21) Boulard, B.; Péron, O.; Chiasera, A.; Ferrari, M.; Jestin, Y. *Proc. SPIE-Int. Soc. Opt. Eng.* **2006**, *6183*, 369−376.
(22) Mortier, M.; Monteville, A.; Patriarche, G.; Mazé, G.; Auzel, F. *Opt. Mater.* **2001**, *16*, 255−267.
(23) Laachir, A.; Perrichon, V.; Badri, A.; Lamotte, J.; Catherine, E.; Lavalley, J. C.; Fallah, J. E.; Hilaire, L.; Le Normand, F.; Quemere, E.; Sauvion, G. N.; Touret, O. *J. Chem. Soc., Faraday Trans.* **1991**, *87*, 1601−1609.
(24) Zhou, X. P.; Wang, S. J.; Weng, W. Z.; Wan, H. L.; Tsai, K. R. *J. Nat. Gas Chem.* **1993**, *4*, 280−289.
(25) Sato, T.; Katakura, T.; Yin, S.; Fujimoto, T.; Yabe, S. *Solid State Ionics* **2004**, *172*, 377−382.
(26) Blümich, B.; Blumler, P.; Jansen, J. *Solid State Nucl. Magn. Reson.* **1992**, *1*, 111−113.
(27) Blumler, P.; Blümich, B.; Jansen, J. *Solid State Nucl. Magn. Reson.* **1994**, *3*, 237−240.
(28) Massiot, D.; Hiet, J.; Pellerin, N.; Fayon, F.; Deschamps, M.; Steuernagel, S.; Grandinetti, P. J. *J. Magn. Reson.* **2006**, *181*, 310−315.

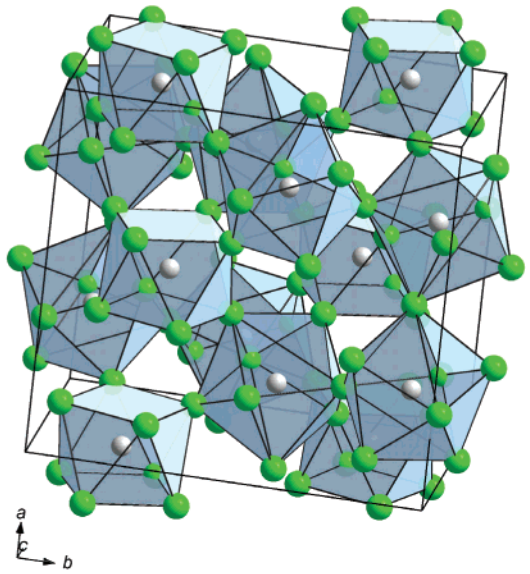


**Figure 1.** Perspective view of $\beta$-$ZrF_4$ structure showing $ZrF_8^{4-}$ square Archimedean antiprism.

projection of the TOP spectra onto the frequency dimension. The $^{19}F$ chemical shift anisotropies were determined from the spinning sidebands intensities according to Herzfeld and Berger.[29] The reconstructions of the one-dimensional MAS spectra (including spinning sidebands) and the TOP processing were both performed with the DMFIT[30] software. The chemical shift tensor is described by three parameters: the isotropic chemical shift, $\delta_{iso}$, the chemical shift anisotropy, $\delta_{aniso}$, and the asymmetry parameter, $\eta$, according to the following formulas:

$$\delta_{iso}\,(ppm) = \frac{\nu - \nu_{ref}}{\nu_{ref}} \times 10^6 = \frac{1}{3}(\delta_{xx} + \delta_{yy} + \delta_{zz}),$$

$$\delta_{aniso}(ppm) = \delta_{zz} - \delta_{iso}, \text{ and } \eta = \frac{\delta_{yy} - \delta_{xx}}{\delta_{aniso}}$$

with the principal components defined in the sequence

$$|\delta_{zz} - \delta_{iso}| \geq |\delta_{xx} - \delta_{iso}| \geq |\delta_{yy} - \delta_{iso}|$$

## Results

The crystal structure of $\beta$-$ZrF_4$ consists of a three-dimensional network of corner-sharing $ZrF_8^{4-}$ square Archimedean antiprism (Figure 1). Each fluorine atom is coordinated by two zirconium atoms.[15] The crystal structure of $\beta$-$ZrF_4$ reported in ref 15 is surprisingly lacking in the Inorganic Crystal Structure Database (ICSD), where there are only reported crystal data from ref 31. Unfortunately, fluorine atomic positions were undetermined in this study. $\beta$-$ZrF_4$ crystallographic data required for discussion are gathered in Table 1 (space group $I2/c$ (No. 15), with unit cell dimensions: $a = 9.57$ Å; $b = 9.93$ Å; $c = 7.73$ Å; and $\beta = 94°28'$). There are seven inequivalent crystallographic fluorine sites, two with a multiplicity of 4 (4d and 4e) and five with 8f multiplicity.

(29) Herzfeld, J.; Berger, A. E. *J. Chem. Phys.* **1980**, *73*, 6021−6030.
(30) Massiot, D.; Fayon, F.; Capron, M.; King, I.; Le Calvé, S.; Alonso, B.; Durand, J.-O.; Bujoli, B.; Gan, Z.; Hoatson, G. *Magn. Reson. Chem.* **2002**, *40*, 70−76.
(31) Zachariasen, W. H. *Acta Cryst.* **1949**, *2*, 388−390.

**Table 1.** Fractional Atomic Coordinates,[15] Fluorine Environments, and F−Zr Bond Lengths (Å) for $\beta$-$ZrF_4$

| atoms | site | symmetry | *x* | *y* | *z* | nearest Zr atoms | F−Zr bond lenghts |
|---|---|---|---|---|---|---|---|
| Zr1 | 4e | 2 | 0 | 0.2148 | 1/4 | | |
| Zr2 | 8f | 1 | 0.2944 | 0.9289 | 0.1278 | | |
| F1 | 4d | −1 | 1/4 | 1/4 | 3/4 | Zr2 | 2.072 |
| | | | | | | Zr2 | 2.072 |
| F2 | 4e | 2 | 0 | 0.598 | 1/4 | Zr2 | 2.132 |
| | | | | | | Zr2 | 2.132 |
| F3 | 8f | 1 | 0.111 | 0.289 | 0.040 | Zr1 | 2.139 |
| | | | | | | Zr2 | 2.148 |
| F4 | 8f | 1 | 0.115 | 0.059 | 0.161 | Zr1 | 2.048 |
| | | | | | | Zr2 | 2.180 |
| F5 | 8f | 1 | 0.212 | 0.526 | 0.104 | Zr2 | 2.031 |
| | | | | | | Zr2 | 2.127 |
| F6 | 8f | 1 | 0.379 | 0.125 | 0.162 | Zr1 | 2.052 |
| | | | | | | Zr2 | 2.118 |
| F7 | 8f | 1 | 0.378 | 0.346 | 0.028 | Zr1 | 2.088 |
| | | | | | | Zr2 | 2.131 |

**Table 2.** Fluorine Environments and F−Ce Bond Lengths (Å) for $CeF_4$

| atoms | site | symmetry | nearest Ce atoms | F−Ce bond lengths |
|---|---|---|---|---|
| F1 | 4e | 2 | Ce1 | 2.271 |
| | | | Ce1 | 2.271 |
| F2 | 8f | 1 | Ce2 | 2.222 |
| | | | Ce1 | 2.237 |
| F3 | 8f | 1 | Ce2 | 2.228 |
| | | | Ce1 | 2.254 |
| F4 | 4d | −1 | Ce1 | 2.213 |
| | | | Ce1 | 2.213 |
| F5 | 8f | 1 | Ce2 | 2.238 |
| | | | Ce1 | 2.269 |
| F6 | 8f | 1 | Ce1 | 2.240 |
| | | | Ce2 | 2.304 |
| F7 | 8f | 1 | Ce1 | 2.200 |
| | | | Ce1 | 2.241 |

$CeF_4$ (ICSD No. 89621, space group $C2/c$ (No. 15), with unit cell dimensions: $a = 12.5883$ Å; $b = 10.6263$ Å; $c = 8.2241$ Å; and $\beta = 126.24°$)[14] is isostructural with $\beta$-$ZrF_4$. The fluorine atom environments are described in Table 2.

Figures 2a and 3a show the $^{19}F$ two-dimensional one-pulse (TOP) MAS NMR spectra of $\beta$-$ZrF_4$ and $CeF_4$, respectively. These spectra contain a large number of intense spinning sidebands that indicate fairly large chemical shift anisotropy values for the fluorine sites of $\beta$-$ZrF_4$ and $CeF_4$. It should be mentioned that spinning frequencies higher than 30 kHz are required to prevent overlap between isotropic lines and spinning sidebands on the $CeF_4$ one-dimensional MAS spectrum that would result in a skewed sideband pattern in the corresponding TOP spectrum.[28] Figures 2b and 3b show the $^{19}F$ experimental and reconstructed "infinite spinning rate" isotropic spectra of $\beta$-$ZrF_4$ and $CeF_4$, respectively, obtained from the projection of the TOP spectra onto the frequency dimension.

The $^{19}F$ isotropic spectrum of $\beta$-$ZrF_4$ is reconstructed (Figure 2b) using seven contributions with relative intensities that are in fine agreement with structural data since five peaks with relative intensity equal to 16.7% and two peaks with relative intensity equal to 8.3% are expected (Tables 1 and 3). It should be noted that this spectrum recorded at 17.6 T clearly shows an improved resolution relative to that previously obtained at a lower magnetic field.[10] The better resolution at high field is due to the greater chemical shift

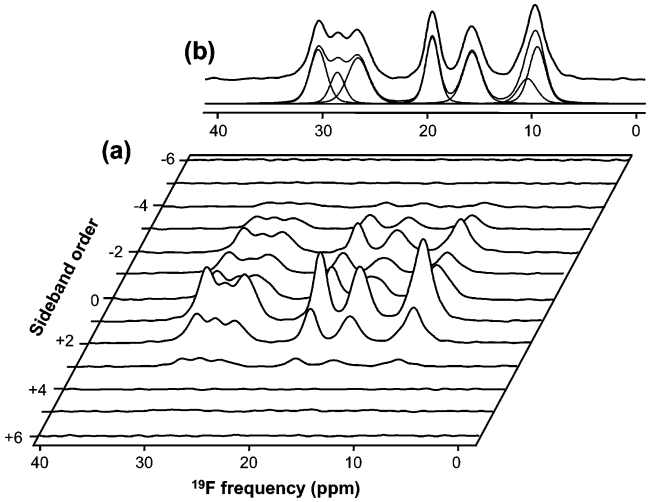


**Figure 2.** (a) $^{19}F$ experimental two-dimensional one-pulse (TOP) MAS spectrum of β-$ZrF_4$ obtained at a magnetic field of 17.6 T and a spinning frequency of 30 kHz. (b) Experimental (top) and reconstructed (bottom) "infinite spinning rate" isotropic spectra of β-$ZrF_4$. The individual contributions to the reconstructed spectrum are shown.

**Table 3.** $\delta_{iso,exp}$ (ppm), $\delta_{aniso}$ (ppm), and $\eta$; Relative Intensities (%) Deduced from $^{19}F$ Isotropic Spectrum Simulation and from One-Dimensional MAS Spectrum Simulation;[a] and Line Attributions and $\delta_{iso,cal}$ (ppm) for β-$ZrF_4$[b]

| line | $\delta_{iso,exp}$ (±0.5) | $\delta_{aniso}$ (±5) | $\eta$ (±0.05) | intensity (±2) | intensity (±2) | attribution | $\delta_{iso,cal}$ |
|---|---|---|---|---|---|---|---|
| 1 | 30.6 | −170 | 0.45 | 16.2 | *16.0* | **F5** | 28.4 |
| 2 | 28.7 | −180 | 0.55 | 8.1 | *8.5* | **F1** | 30.4 |
| 3 | 26.7 | −170 | 0.55 | 17.3 | *17.8* | **F6** | 26.4 |
| 4 | 19.6 | −170 | 0.4 | 16.0 | *15.7* | F7 | 18.6 |
| 5 | 15.8 | −165 | 0.4 | 17.0 | *16.0* | F4 | 17.7 |
| 6 | 10.4 | −160 | 0.3 | 8.3 | *7.7* | **F2** | 11.6 |
| 7 | 9.5 | −175 | 0.3 | 17.1 | *18.3* | **F3** | 8.2 |

[a] In italics. [b] Unambiguous attributions are in bold.

dispersion (in frequency units). The chemical shift anisotropies (CSA) of the seven individual contributions were determined from the spinning sideband intensities.[29] The obtained chemical shift anisotropy values range between −160 and −180 ppm, and the $\eta$ values range between 0.3 and 0.55 (Table 3), in agreement with the rhombic fluorine site symmetries (Table 1). The simulation of the one-dimensional MAS spectrum of β-$ZrF_4$ using these CSA parameters is shown in Figure 4. The relative intensities of the seven $^{19}F$ NMR resonances obtained from the simulation of the conventional one-dimensional MAS spectrum are in good agreement with those determined from the "infinite spinning frequency" isotropic spectrum. The distinction between fluorine sites with different multiplicities is unambiguous, allowing us to definitely assign lines 2 and 6 to the F1 and/or F2 fluorine sites as these sites are expected to be half as abundant as the five other fluorine sites in the structure (Table 1). At this stage, there is no way a priori of choosing between F1 and F2 for these two peaks. The assignment of lines 2 and 6 to less intense resonances differ with those obtained in ref 10, where reconstruction was done by analyzing only the isotropic lines of the one-dimensional MAS lower resolution spectrum.

As for β-$ZrF_4$, the $^{19}F$ "infinite spinning frequency" isotropic spectrum obtained from the projection of the TOP

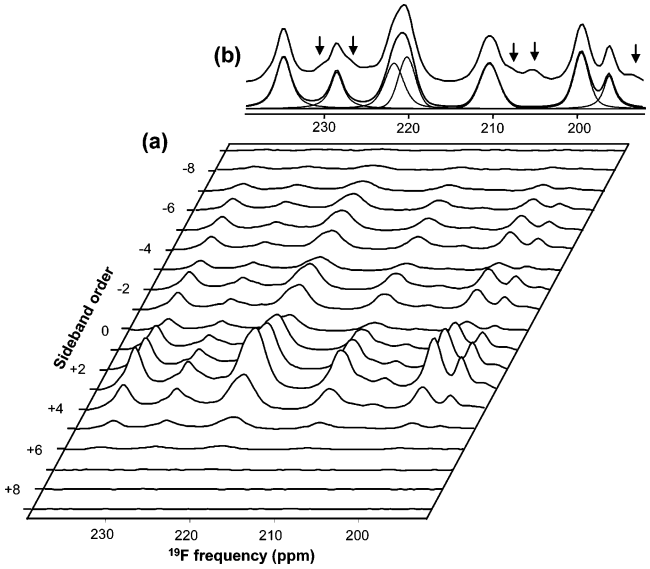


**Figure 3.** (a) $^{19}F$ experimental two-dimensional one-pulse (TOP) MAS spectrum of $CeF_4$ obtained at a magnetic field of 17.6 T and a spinning frequency of 34 kHz. (b) Experimental (top) and reconstructed (bottom) "infinite spinning rate" isotropic spectra of $CeF_4$. The individual contributions to the reconstructed spectrum are shown. The arrows point out resonances attributed to unidentified impurity.

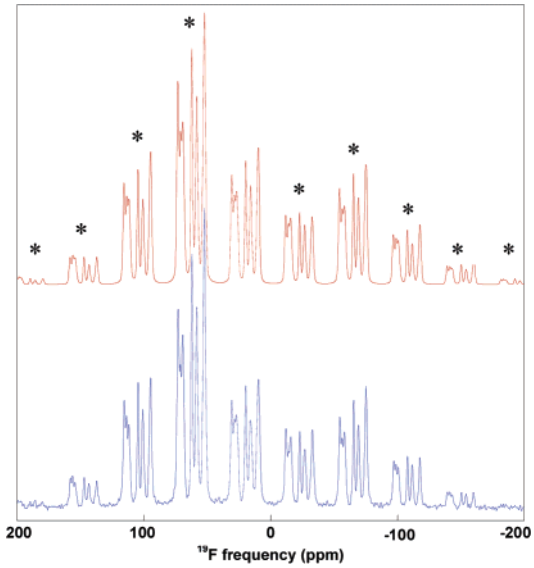


**Figure 4.** Experimental (bottom) and reconstructed (top) $^{19}F$ one-dimensional MAS NMR spectra of β-$ZrF_4$ obtained at a magnetic field of 17.6 T and a spinning frequency of 30 kHz. Spinning sidebands are marked by asterisks.

spectrum of $CeF_4$ can be reconstructed with seven peaks (Figure 3b) with relative intensities in agreement with structural data (Tables 2 and 4). The associated $^{19}F$ chemical shift anisotropies determined from the spinning sideband intensities[29] are gathered in Table 4. It should be noted that the $^{19}F$ experimental isotropic spectrum of $CeF_4$ exhibits some extra lines of weak intensities (Figure 3b). These extra lines were attributed to an impurity since their relative intensities (as compared to the intensities of the resonances attributed to $CeF_4$) differ from one sample to another. Moreover, their relative intensities are lower than 8%, and they cannot be attributed to fluorine sites of $CeF_4$ according to the expected site multiplicities. This impurity, which is

**Table 4.** $\delta_{iso,exp}$ (ppm), $\delta_{aniso}$ (ppm), and $\eta$; Relative Intensities (%) Deduced from $^{19}F$ Isotropic Spectrum Simulation and from One-Dimensional MAS Spectrum Simulation;[a] and Line Attributions and $\delta_{iso,cal}$ (ppm) for $CeF_4$[b]

| line | $\delta_{iso,exp}$ (±0.5) | $\delta_{aniso}$ (±7) | $\eta$ (±0.05) | intensity (±2) | intensity (±2) | attribution | $\delta_{iso,cal}$ |
|---|---|---|---|---|---|---|---|
| 1 | 235.0 | −390 | 0.3 | 16.7 | *15.2* | **F7** | 229.5 |
| 2 | 228.6 | −410 | 0.3 | 11.2 | *10.6* | **F4** | 233.9 |
| 3 | 221.8 | −390 | 0.25 | 16.9 | *16.4* | **F2** | 223.8 |
| 4 | 220.3 | −390 | 0.25 | 15.5 | *16.8* | **F3** | 217.0 |
| 5 | 210.4 | −380 | 0.2 | 15.2 | *17.5* | **F5** | 209.5 |
| 6 | 199.5 | −370 | 0.15 | 16.3 | *15.4* | **F6** | 199.0 |
| 7 | 196.2 | −370 | 0.1 | 8.2 | *8.1* | **F1** | 199.2 |

[a] In italics. [b] Unambiguous attributions are in bold.

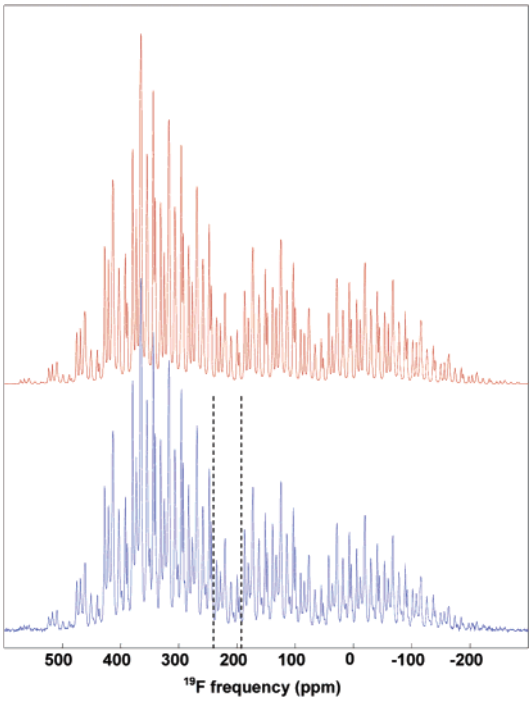


**Figure 5.** Experimental (bottom) and reconstructed (top) $^{19}F$ one-dimensional MAS NMR spectra of $CeF_4$ obtained at a magnetic field of 17.6 T and a spinning frequency of 34 kHz. The dashed lines delimit the isotropic resonance range.

not detected on the X-ray powder pattern, likely would be a cerium IV oxy-(hydroxy)-fluoride since the observed $\delta_{iso}$ values are close to the $CeF_4$ ones and are then characteristic of fluorine ions with $Ce^{4+}$ ions as nearest neighbors. The agreement between expected and experimental relative intensities is not as fine as for $\beta$-$ZrF_4$, certainly due to the presence of the impurity. Nevertheless, the distinction between fluorine sites with different multiplicities is unambiguous. Lines 2 and 7 can be easily assigned to F1 and/or F4 fluorine sites, as these sites are expected to be half as abundant as the five other fluorine sites in the structure (Table 2). The CSA values ranging between −370 and −410 ppm (Table 4) are larger than those measured for $\beta$-$ZrF_4$ fluorine sites. As for $\beta$-$ZrF_4$, the $\eta$ values ranging between 0.1 and 0.3 (Table 4) are all different from zero, in agreement with the rhombic fluorine site symmetries (Table 2). The simulation of the one-dimensional MAS spectrum of $CeF_4$ using these CSA parameters is shown in Figure 5. The relative intensities of the seven $^{19}F$ NMR resonances obtained from the simulation of the conventional one-dimensional MAS spectrum are in good agreement with those determined from the "infinite spinning frequency" isotropic spectrum.

**Table 5.** $\alpha_l$ ($Å^{-1}$), $d_0$ (Å), and $\sigma_{l_0}$ (ppm) Parameters Before and After[a] Refinement for $\beta$-$ZrF_4$ and $CeF_4$

| compound | $\alpha_l$ | | $d_0$ | | $\sigma_{l_0}$ | |
|---|---|---|---|---|---|---|
| $\beta$-$ZrF_4$ | 3.26 | *0.99* | 2.105 | *2.109* | −155.8 | *−155.0* |
| $CeF_4$ | *3.15* | *1.18* | *2.243* | *2.245* | *−253.9* | *−252.8* |

[a] In italics.

## Discussion

The superposition model for $^{19}F$ isotropic chemical shift calculation was proposed by Bureau et al.[11] for ionic fluorides. In this model, the $^{19}F$ isotropic chemical shift is considered to be a sum of one constant diamagnetic term and several paramagnetic contributions from the $l$ neighboring cations and is calculated according to the main following formula:[11]

$$\delta_{iso/C_6F_6} = -127.1 - \sum_l \sigma_l \text{ and } \sigma_l = \sigma_{l_0} \exp[-\alpha_l(d - d_0)],$$

$$\text{which corresponds to } \delta_{iso/CFCl_3} = -291.3 - \sum_l \sigma_l$$

where $d_0$ is the characteristic F−M distance that is taken equal to the bond length in the related basic fluoride, and $\sigma_{l_0}$ is the parameter that determines the order of magnitude of the cationic paramagnetic contribution to the shielding and was deduced from measurements in the related basic fluoride where $\delta_{iso/CFCl_3} = -291.3 - n\sigma_{l_0}$ ($n$ is the coordination number of the fluorine atom).

The first step, using this model, is to determine $\alpha_l$. For atoms whose atomic radial wave functions are known, $\alpha_l$ was deduced from the behavior of the cation isotropic paramagnetic contribution $\bar{\sigma}^p$ (see formula in Appendix A of ref 11) calculated for several $d$ distances on the basis of Ramsey's theory[32] with molecular orbitals obtained by Löwdin's orthogonalization method.[33] A linear relation between $\alpha_l$ and the ionic radius $r_l$ of the ligand $l$ has been established: $\alpha_1 = -0.806r_1 + 4.048$. This formula was applied to cations for which radial wave functions are unknown. As is the case for $Zr^{4+}$ and $Ce^{4+}$ cations, we use it to calculate the corresponding initial $\alpha_l$ parameters (Table 5). The $Zr^{4+}$ and $Ce^{4+}$ crystal radii are taken equal to 0.98 and 1.11 Å, respectively.[34]

The second step consists in determining $d_0$ and $\sigma_{l_0}$ values. Since the structure of $\beta$-$ZrF_4$ and $CeF_4$ contains several distinct crystallographic fluorine sites with several different F−Zr distances and $\delta_{iso}$ values, this determination is not as straighforward as for basic fluorides containing a single fluorine crystallographic site.[11] $d_0$ and $\sigma_{l_0}$ values were determined for both atoms, considering weighted average values of $d_0$ and $\delta_{iso}$ (Table 5).

The last step is to define the number of neighboring cations $M$ whose contributions have to be taken into account. As

(32) Ramsey, N. F. *Phys. Rev.* **1950**, *78*, 699−703.
(33) Löwdin, P. Ö. *Adv. Phys.* **1956**, *5*, 1−172.
(34) Shannon, R. D. *Acta Crystallogr., Sect. A* **1976**, *32*, 751−767.

was previously done for basic fluorides, only the first fluorine coordination sphere was considered in the calculation.[11] The next nearest neighboring cations in $\beta$-$ZrF_4$ and $CeF_4$ are at distances larger than 3.75 and 4.0 Å, respectively, and it was previously shown that it is needless to perform calculations with sphere radii larger than 3.5 Å.[12]

The values obtained with this model are compared with the experimental results for $\beta$-$ZrF_4$ and $CeF_4$. The calculated and experimental isotropic chemical shifts are then matched, having regard for the first attribution based on the relative intensities, to minimize the difference: $\Delta\delta_{iso} = \delta_{iso,exp} - \delta_{iso,cal}$. The obtained rms deviations of 19 and 22 ppm for $\beta$-$ZrF_4$ and $CeF_4$, respectively, are too large to perform any attribution. Therefore, a minimization of the sum $S = \sum(\delta_{iso,cal} - \delta_{iso,exp})^2$ was carried out with $\alpha_l$, $d_0$, and $\sigma_{l_0}$ as adjustable parameters. A new parameter set is obtained, and, if necessary, the line attribution is modified, with respect to the relative intensities, to keep the difference between calculated and experimental $\delta_{iso}$ at a minimum. Usually, this process is repeated until the line attribution remains unchanged, but in this study, only one new attribution of the NMR lines was performed: permutation between F4 and F7 attributions for $\beta$-$ZrF_4$. The rms deviations of 1.5 and 3.5 ppm were achieved for $\beta$-$ZrF_4$ and $CeF_4$, respectively. The calculated isotropic chemical shift values and the corresponding line attributions are collected in Tables 3 and 4 for $\beta$-$ZrF_4$ and $CeF_4$, respectively. It should be noted that the assignment of the F4 and F7 resonances in $\beta$-$ZrF_4$ remains ambiguous since the difference between their calculated $^{19}F$ isotropic chemical shifts is small, within the rms deviation of 1.5 ppm (Table 3). Nevertheless, our results lead to a more detailed attribution of the $^{19}F$ resonances to the fluorine sites in $\beta$-$ZrF_4$ than that previously proposed.[10] This is certainly due to the fact that the F−Zr bond lengths used in ref 10 were clearly inaccurate.

A comparison between initial and refined parameters (Table 5) of the superposition model shows that the only sensitive parameter is $\alpha_l$, which describes the behavior of the paramagnetic contribution with the F−M distance. The decrease for the $\alpha_l$ parameter may be correlated with deviation from the purely ionic model[12] for F−Zr and F−Ce bonds. In other words, the orbital overlap between F and Zr or Ce atoms is larger than in a purely ionic model.

## Conclusion

High magnetic field and high spinning frequency one- and two-dimensional one-pulse $^{19}F$ MAS NMR spectra were recorded for the two isostructural compounds $\beta$-$ZrF_4$ and $CeF_4$. From the reconstruction of these experimental spectra, the $^{19}F$ chemical shift parameters of the seven resonances corresponding to the seven crystallographic inequivalent fluorine sites in the $\beta$-$ZrF_4$ and $CeF_4$ structures were determined. The attributions of the $^{19}F$ resonances to the various fluorine sites were performed using the superposition model initially proposed by Bureau et al.,[11] which was applied for the first time on basic fluorides containing several fluorine sites. A good agreement is obtained between experimental and calculated isotropic chemical shift values, the rms deviation values being equal to 1.5 and 3.5 ppm for $\beta$-$ZrF_4$ and $CeF_4$, respectively.

**Acknowledgment.** We thank J.-P. Laval, from the SPCTS, CNRS UMR 6638, Université de Limoges, who kindly supplied us with ref 15.

IC061339A